

Measurement method for the nuclear anapole moment of laser trapped alkali atoms

E. Gomez, S. Aubin*, and G. D. Sprouse

Dept. of Physics and Astronomy, State University of New York at Stony Brook, Stony Brook, NY 11794-3800, U.S.A.

L. A. Orozco

Dept. of Physics, University of Maryland, College Park, MD 20742-4111

D. P. DeMille

Dept. of Physics, Yale University, New Haven, CT 06520-8120, U.S.A.

(May 23, 2019)

Weak interactions within a nucleus generate a nuclear spin dependent parity violating electromagnetic moment; the anapole moment. In heavy nuclei, the anapole moment is the dominant contribution to spin-dependent atomic parity violation. We analyze a method to measure the nuclear anapole moment through the electric dipole transition it induces between hyperfine states of the ground level. The method requires tight confinement of the atoms to position them at the anti-node of a standing wave driving the anapole-induced E1 transition. We explore the necessary limits in the number of atoms, excitation fields, trap type, interrogation method, and systematic tests necessary for such measurements in francium, the heaviest alkali.

I. INTRODUCTION

Parity nonconservation (PNC) in atoms comes from two types of interaction: Nuclear spin independent and nuclear spin dependent [1]. Nuclear spin dependent PNC occurs in three ways [2,3]: An electron interacts weakly with a single valence nucleon (nucleon axial-vector current $A_n V_e$), the nuclear chiral current created by weak interactions between nucleons (anapole moment), and the combined action of the hyperfine interaction and the spin-independent Z^0 exchange interaction from nucleon vector currents ($V_n A_e$). [4,5].

Zel'dovich first proposed the existence of the nuclear anapole moment in 1957 [6]. Vetter *et al.* [7] obtained a limit for its value in thallium, and it was measured with an accuracy of 15% through the hyperfine dependence of atomic parity nonconservation in cesium by Wood *et al.* [8,9]. Previous studies have proposed measuring the anapole moment more directly through hyperfine transitions in alkali atoms [10–14]. In this paper, we study the feasibility of measuring the anapole moment through the electric dipole transitions it induces between the hyperfine levels of the ground state in alkali atoms held in a dipole trap. Since the anapole moment scales as $Z^{2/3}$ and the matrix element scales as Z^2 , with Z the atomic number, we focus our study primarily on francium isotopes, the heaviest of the alkali atoms [15]. Recent work related to time-reversal invariance tests in traps [16,17] points to the many potential advantages of combining traps with tests of fundamental symmetries, but also highlights the

systematics errors present in such measurements, indicating further work is needed.

The organization of the paper is as follows: Section II gives the theoretical background for the nuclear anapole moment, section III explains the proposed measurement method, section IV presents an analysis of the systematic effects, and section V contains the conclusions.

II. THEORETICAL BACKGROUND

Parity violating atomic transitions are generated primarily by the exchange of weak neutral currents between electrons and nucleons. These currents can be of two kinds, depending on whether the electron or the nucleon gives the axial vector current. Assuming an infinitely heavy nucleon without radiative corrections, the hamiltonian is [18]

$$H = \frac{G}{\sqrt{2}} (\kappa_{1i} \gamma_5 - \kappa_{nsd,i} \sigma_{\mathbf{n}} \cdot \boldsymbol{\alpha}) \delta(\mathbf{r}), \quad (1)$$

where $G = 10^{-5} \text{ m}_p^{-2}$ is the Fermi constant, m_p is the proton mass, γ_5 and $\boldsymbol{\alpha}$ are Dirac matrices, $\sigma_{\mathbf{n}}$ are Pauli matrices, and κ_{1i} and $\kappa_{nsd,i}$ (nuclear spin dependent) with $i = p, n$ for a proton or a neutron are constants of the interaction. At tree level $\kappa_{nsd,i} = \kappa_{2i}$, and in the standard model these constants are given by

*Present address: Department of Physics, University of Toronto, Ontario, Canada

$$\begin{aligned}\kappa_{1p} &= \frac{1}{2}(1 - 4\sin^2\theta_W), \kappa_{1n} = -\frac{1}{2}, \\ \kappa_{2p} &= -\kappa_{2n} = \kappa_2 = -\frac{1}{2}(1 - 4\sin^2\theta_W)\eta,\end{aligned}\quad (2)$$

with $\sin^2\theta_W \sim 0.23$ the Weinberg angle and $\eta = 1.25$. κ_{1i} (κ_{2i}) represents the coupling between nucleon and electron currents when the electron (nucleon) is the axial vector.

In an atom, we must add the contribution from Eq. 1 for all the nucleons. It is convenient to work in the approximation of shell model with a single valence nucleon of unpaired spin. The first term of Eq. 1 gives a contribution that is independent of the nuclear spin and proportional to the weak charge $Q_W = 2(\kappa_{1p}Z + \kappa_{1n}N)$, with N the number of neutrons. For the standard model values, the weak charge is almost equal to $-N$. The second term is nuclear spin dependent and due to the pairing of nucleons its contribution has smaller dependence on Z . The result for this second term is [19]

$$H_{PNC}^{nsd} = \frac{G}{\sqrt{2}} \frac{K \mathbf{I} \cdot \boldsymbol{\alpha}}{I(I+1)} \kappa_{nsd} \delta(r), \quad (3)$$

where $K = (I+1/2)(-1)^{I+1/2-l}$, l is the nucleon orbital angular momentum, I is the nuclear spin. The terms proportional to the anomalous magnetic moment of the nucleons and the electrons have been neglected.

The interaction constant is given now by [19]

$$\kappa_{nsd} = \kappa_a - \frac{K-1/2}{K} \kappa_2 + \frac{I+1}{K} \kappa_{Q_W}, \quad (4)$$

where $\kappa_2 \sim -0.05$ from Eq. 2 is the tree level approximation, and we have two corrections, the effective constant of the anapole moment κ_a and κ_{Q_W} that is generated by the nuclear spin independent part of the electron nucleon interaction together with the hyperfine interaction. Flambaum and Murray show that [19]

$$\begin{aligned}\kappa_a &= \frac{9}{10} g \frac{\alpha\mu}{m_p \tilde{r}_0} \mathcal{A}^{2/3}, \\ \kappa_{Q_W} &= -\frac{1}{3} Q_W \frac{\alpha\mu_N}{m_p \tilde{r}_0} \mathcal{A}^{2/3},\end{aligned}\quad (5)$$

where α is the fine structure constant, μ and μ_N are the magnetic moment of the external nucleon and of the nucleus respectively in nuclear magnetons, $\tilde{r}_0 = 1.2$ fm is the nucleon radius, $\mathcal{A} = Z + N$, and g gives the strength of the weak nucleon-nucleon potential with $g_p \sim 4$ for protons and $0.2 < g_n < 1$ for neutrons [18]. Since both κ_a and κ_{Q_W} scale as $\mathcal{A}^{2/3}$, the interaction is stronger in heavier atoms. The anapole moment is the dominant contribution to the interaction in heavy atoms, for example in ^{209}Fr , $\kappa_a/\kappa_{Q_W} \simeq 15$. From now on we will assume $\kappa_{nsd} = \kappa_a$ unless stated otherwise.

A. The anapole moment

The anapole moment of a nucleus is a parity non conserving (PNC), time reversal conserving moment that arises from weak interactions between the nucleons (see the recent review by Haxton and Wieman [4]). It can be detected in a PNC electron-nucleus interaction and reveals itself in the spin dependent part of the PNC interaction. Wood *et al.* [8,9] measured the anapole moment of ^{133}Cs by extracting the dependence of atomic PNC on the hyperfine energy levels involved, and consequently nuclear spin. The measurement shows that atomic PNC is a unique probe for neutral weak interactions inside the nucleus, which otherwise remain hidden by much larger electromagnetic charged currents [20].

The anapole moment is defined by

$$\mathbf{a} = -\pi \int d^3r r^2 \mathbf{J}(\mathbf{r}), \quad (6)$$

with \mathbf{J} the electromagnetic current density. The anapole moment in francium arises mainly from the weak interaction between the valence nucleons and the core. Flambaum, Khriplovich and Sushkov [3] by including weak interactions between nucleons in their calculation of the nuclear current density, estimate the anapole moment from Eq. 6 of a single valence nucleon to be

$$\mathbf{a} = \frac{1}{e} \frac{G}{\sqrt{2}} \frac{K \mathbf{j}}{j(j+1)} \kappa_a = C^{an} \mathbf{j}, \quad (7)$$

where j is the nucleon angular momentum. These values correspond to the nuclear values for the case of a single valence nucleon. The calculation is based on the shell model for the nucleus, under the assumption of homogeneous nuclear density and a core with zero angular momentum leaving the valence nucleon carrying all the angular momentum.

B. Calculations of anapole moments of francium isotopes

We have used Eqs. 5 and 7 to estimate the anapole moments of the light francium isotopes. In even-neutron isotopes, the unpaired valence proton generates the anapole moment, whereas in the odd-neutron isotopes both the unpaired valence proton and neutron participate. We then have an unpaired $h_{9/2}$ proton for all the isotopes and an $f_{5/2}$ neutron for the odd-neutron isotopes. In the latter case, one must add vectorially the contributions from both the proton and the neutron to obtain the anapole moment

$$\mathbf{a} = \frac{C_p^{an} \mathbf{j}_p \cdot \mathbf{I} + C_n^{an} \mathbf{j}_n \cdot \mathbf{I}}{I^2} \mathbf{I}, \quad (8)$$

with $C_i^{an} \mathbf{j}_i$ the anapole moment for a single valence nucleon i in a shell model description as given by Eq. 7,

with $j_p=9/2$ and $j_n=5/2$. Figure 1 shows the predicted coupling strength of the anapole moment, κ_a , for a string of francium isotopes (available at the Superconducting LINAC of Stony Brook [15]) using $g_n=1$.

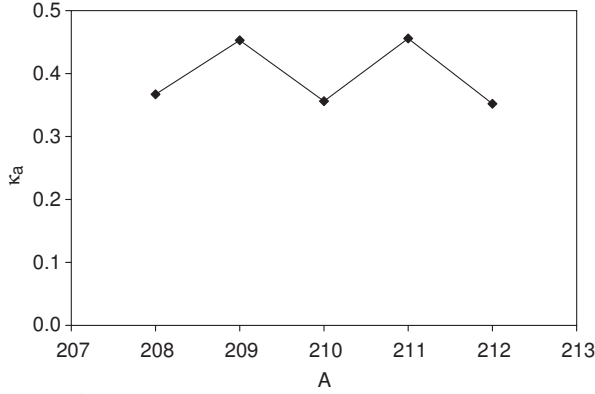


FIG. 1. Anapole moment effective constant for the different isotopes of francium.

C. Perturbation theory

The anapole moment induces a small mixing of electronic states of opposite parity. According to first order perturbation theory, the effect of the anapole moment Hamiltonian on the ground state hyperfine levels is

$$|sFm\rangle = |sFm\rangle + \sum_{F'm'} \frac{\langle pF'm' | \mathbf{H}_a | sFm \rangle}{E_p - E_s} |pF'm'\rangle, \quad (9)$$

where E_p, E_s are the energies of the p and s states respectively and

$$\mathbf{H}_a = |e| \boldsymbol{\alpha} \cdot \mathbf{a} \delta(\mathbf{r}), \quad (10)$$

is the anapole moment Hamiltonian from Eq. 3 and \mathbf{a} the anapole moment from Eq. 7. Calculating the matrix element in Eq. 9, we obtain [18]

$$\langle pF'm' | \mathbf{H}_a | sFm \rangle = i \frac{\xi Z^2 R}{(\varrho_s \varrho_p)^{3/2}} \frac{2\gamma + 1}{3} \frac{\kappa_a K R y}{I(I+1)} \times (F(F+1) - I(I+1) - 3/4) \delta_{F,F'} \delta_{m,m'}, \quad (11)$$

with $\xi = G m_e^2 \alpha^2 / \sqrt{2} \pi = 3.651 \times 10^{-17}$, m_e the electron mass, ϱ_s and ϱ_p the effective principal quantum number for the s and p electronic states, $\gamma = \sqrt{(J+1/2)^2 - Z^2 \alpha^2}$, J the angular momentum, and $R y$ the Rydberg. The relativistic enhancement factor R is given by

$$R = 4(a_0/2Zr_0)^{2-2\gamma} / \Gamma^2(2\gamma+1), \quad (12)$$

with a_0 the Bohr radius and $r_0 = \tilde{r}_0 A^{1/3}$ the size of the nucleus.

The anapole moment mixes only states with the same F and m . For ^{209}Fr ground state, we obtain

$$|\overline{sFm}\rangle = |sFm\rangle - i 5.9 \times 10^{-13} \kappa_a \times (F(F+1) - 25.5) |pFm\rangle. \quad (13)$$

The mixing coefficient is imaginary due to time reversal symmetry. In practice, the mixing is measured through the transition amplitude it induces. The presence of external electric and magnetic fields further modifies the mixing and must also be included. In the measurement considered in this paper, the transition amplitude for ^{209}Fr between the hyperfine level $F=4$, $m=0$ to $F=5$, $m=-1$ with a microwave electric field of 476 V/cm oscillating along the x -axis (Fig. 2) and a static magnetic field of 1553 Gauss along the z -axis is

$$A_{E1}/\hbar = \langle \bar{f} | -e \mathbf{E} \cdot \mathbf{r} | i \rangle / \hbar = 0.01 i \left[\frac{E}{476 \text{ V/cm}} \right] \left[\frac{\kappa_a}{0.45} \right] \text{ rad}. \quad (14)$$

A more accurate result can be obtained with the use of many-body methods [5,21,22]. The electric field correspond to the expected one for our setup and the static magnetic field is the one required to reduce the sensitivity of the measurement to magnetic field fluctuations

III. MEASUREMENT STRATEGY

We propose a measurement of the nuclear anapole moment by direct excitation of the microwave E1 transition between the ground hyperfine states of an alkali atom. The transition is parity forbidden, but is allowed by the anapole induced mixing of opposite parity states. The general approach has been suggested and followed in the past [10–12,23,24]. We modify the suggestion of Fortson [20] for atomic PNC to use an ion placed at the anti-node of a standing optical wave. We place many trapped atoms at the anti-node of a standing microwave field, so that the stability requirements on the interrogated sample are relaxed. Nevertheless, the atoms must be well localized within the anti-node of the standing wave (microwave frequency $\nu_m \sim 45$ GHz and wavelength $\lambda_m \sim 6.6$ mm for francium).

In the case of francium, we prepare the atomic sample in the following manner. Francium atoms from the Superconducting LINAC at Stony Brook are initially trapped in a high efficiency magneto-optical trap (MOT) [25], and then transferred to a second MOT in a separate chamber by means of a push beam. We then load the atoms into a dipole trap located at the electric field anti-node of a standing wave in a microwave cavity. Given all the constraints for preparation and transfer of the francium atoms, we will use a Fabry-Perot configuration for the microwave cavity.

Once the atoms are in the dipole trap we pump them into a single Zeeman sublevel. We prepare a coherent superposition of the hyperfine ground states with a Raman

pulse of amplitude A_R and duration t_R . Simultaneously we drive the E1 transition of amplitude A_{E1} with the cavity microwave field and then measure the population in the upper hyperfine level (normalized by the total number of atoms (N)) through a cycling transition. At the end of each sequence the excited state population is given by

$$\Xi_{\pm} = N|c_e|^2 = N \sin^2 \left(\frac{(A_R \pm A_{E1})t_R}{2\hbar} \right), \quad (15)$$

where c_e is the upper hyperfine amplitude. The sign depends on the handedness of the coordinate system defined by the external fields as explained below. We measure the population transfer for both signs and define the signal as

$$\begin{aligned} \mathcal{S} = \Xi_+ - \Xi_- &= N \sin \left(\frac{A_R t_R}{\hbar} \right) \sin \left(\frac{A_{E1} t_R}{\hbar} \right) \\ &\simeq N \sin \left(\frac{A_R t_R}{\hbar} \right) \left(\frac{A_{E1} t_R}{\hbar} \right), \end{aligned} \quad (16)$$

where for the last step it was assumed a small A_{E1} . Having the E1 transition amplitude we can work our way back and obtain the interaction constant κ_{nsd} .

A. Signal to noise ratio

The choice for the value of A_R has to take into account the different sources of noise on the measurement. The signal is maximized for a $\pi/2$ Raman pulse. The measurement of the upper hyperfine state population collapses the state of each atom into one of the two hyperfine levels. The collapse distributes the atoms binomially between the two hyperfine levels and leads to an uncertainty in the measured excited state fraction called projection noise [26]. The projection noise is given by

$$\mathcal{N}_P = \sqrt{N|c_e|^2(1 - |c_e|^2)}. \quad (17)$$

Note that the projection noise is zero when all the atoms are in one of the hyperfine levels. We can select the Raman pulse to reduce the projection noise at the expense of reducing also the signal. If one includes other sources of noise such as the photon shot noise, that goes as $\sqrt{N|c_e|^2}$, then the optimum operating value for the Raman pulse is still around a $\pi/2$ pulse. For a projection noise limited measurement, the signal-to-noise ratio is

$$\frac{\mathcal{S}}{\mathcal{N}_P} = 2 \frac{A_{E1} t_R}{\hbar} \sqrt{N}. \quad (18)$$

We want as many atoms as possible to increase the signal to noise ratio. Taking A_{E1} from Eq. 14 and $t_R = 1$ s (a reasonable assumption for the expected coherence time

as explained below) we need 300 atoms for a 3% measurement after 10^4 cycles. With more atoms it will be easier to study all the systematic effects. It seems reasonable to expect a sample of 10^6 francium atoms, which will give a signal to noise ratio of 20. A_{E1} depends linearly on κ_a , the constant we are trying to measure, so using heavy atoms such as francium will increase the signal to noise ratio.

While measurements in francium benefit from a large A_{E1} , large atomic samples of other alkalis are easily prepared. For example, while the anapole-induced parity mixing is a factor of 10 smaller in cesium than in francium, a competitive measurement with the same signal-to-noise requires a sample population 100 times larger or $N = 10^8$ for the same strength driving field. While the fundamental signal-to-noise indicates the inherent trade-offs between different alkali species, technical noise must also be considered. Having a large A_{E1} minimizes the relative effect of technical noise sources.

At the end the noise will be dominated by technical noise. The measurement is specially sensitive to detunings. The effect can be reduced by increasing the Raman pulse to an odd multiple of a $\pi/2$ pulse. This does not change any of the results obtained so far.

B. Apparatus setup

Figure 2 shows a simplified diagram of the proposed apparatus in the ideal-case situation. The atoms (located at the origin) are prepared in a particular Zeeman sub-level $|F, m\rangle$. We apply an static magnetic field $\mathbf{B} = B\hat{\mathbf{z}}$. The atoms are excited by an standing-wave microwave electric field $\mathbf{E}(t) = E \cos(\nu_m t + \psi) \cos(k_m y) \hat{\mathbf{x}}$. The microwave frequency ν_m is tuned to the Zeeman-shifted hyperfine transition frequency ν_0 . The microwave magnetic field \mathbf{M} is deliberately aligned along \mathbf{B} ; since (for a perfect standing wave) \mathbf{M} is out of phase with \mathbf{E} , we thus have $\mathbf{M}(t) = M \sin(\nu_m t + \psi) \sin(k_m y) \hat{\mathbf{z}}$, with $M = E$ in cgs units. As we discuss below, proper alignment of \mathbf{M} and positioning of the standing-wave node is critical for suppressing systematic effects and line-broadening mechanisms. The Raman transition is driven by two plane-wave optical fields, $\mathbf{E}_{R1}(t) = E_{R1} \cos(\omega_R t + \phi_R) \hat{\mathbf{x}}$ and $\mathbf{E}_{R2}(t) = E_{R2} \cos((\omega_R + \nu_m)t + \phi_R) \hat{\mathbf{z}}$. We assume that the Raman carrier frequency ω_R is detuned sufficiently far from optical resonance that only the vector part of the Raman transition amplitude ($\mathbf{V} \propto i\mathbf{E}_{R1} \times \mathbf{E}_{R2}$) is non-negligible [27]; that is, we ignore the tensor part of the Raman amplitude. In the rotating wave approximation the Raman amplitude is given by

$$A_R = \frac{E_{R1} E_{R2}}{4} \sum_{k'} \left(\frac{\langle f | -e\hat{\mathbf{x}} \cdot \mathbf{r} | k' \rangle \langle k' | -e\hat{\mathbf{z}} \cdot \mathbf{r} | i \rangle}{E_{k'} - E_s - \hbar\omega_R} \right) \quad (19)$$

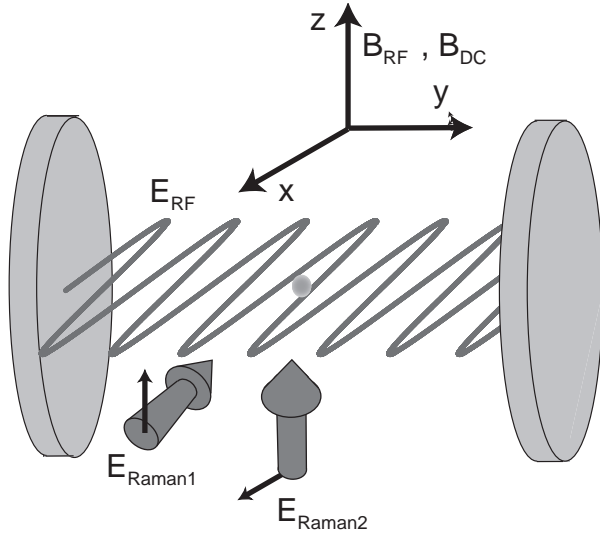


FIG. 2. Schematic setup of the apparatus. The microwave cavity axis is along the y -axis. The microwave electric field inside the cavity oscillates along the x -axis. The two Raman laser beams are polarized along the x -axis and z -axis, respectively. The microwave magnetic field and the static magnetic field are both directed along the z -axis. A dipole trap (not shown) holds the atoms at the anti-node of the microwave electric field.

The various electric and magnetic fields of the apparatus define a coordinate system related to the measured rate Ξ_{\pm} . The transition rate Ξ_{\pm} depends on three vectors: The polarization of the E1 transition, the polarization of the Raman transition (\mathbf{V}), and the static magnetic field \mathbf{B} which defines magnetization of the atoms. We combine these three vectors to produce the pseudoscalar $\mathbf{i}(\mathbf{E} \times (\mathbf{E}_{R1} \times \mathbf{E}_{R2}) \cdot \mathbf{B})$ proportional to the measured quantity.

The time varying fields must be all phase locked with respect to each other. The above pseudoscalar indicates the methods for changing the handedness of the measurement, a single reversal of any of the fields will change the sign of the interference term of Ξ_{\pm} .

In summary we have the following reversals at our disposal:

- 1.- Magnetic field reversal (β reversal).
- 2.- A shift of π in the relative phase between the E1 and the Raman fields (s reversal).

Reversing the magnetic field will also reverse the Zeeman sublevels. In order to reach the correct Zeeman sublevel the state preparation has to be inverted, meaning that σ^+ light will go into σ^- and viceversa. Everything else will remain the same, including the point of operation of the static magnetic field and the frequency of the microwave cavity.

C. Magnetic field

The stability of the static magnetic field, B_{DC} , influences the precision of the measurement. We want to drive E1 transitions between two particular Zeeman sublevels, $|F = 4, m_1\rangle \rightarrow |F = 5, m_2\rangle$. The Rabi frequencies, Ω_R and Ω_{E1} , depend on the detuning of the driving field from the energy difference of these two states. While the frequencies of the exciting fields can be well controlled, the energy difference of the Zeeman states is determined primarily by the static magnetic field.

The design of the experiment must minimize the sensitivity to magnetic field fluctuations. We can choose the static magnetic field such that the energy separation between levels goes through a minimum. At the minimum, the energy separation depends quadratically on the magnetic field. We use the Zeeman sublevels which give the smallest quadratic dependence. The mixing of levels due to the magnetic field needs to be taken into account to calculate the E1 amplitude. Table I lists the appropriate Zeeman sublevels and magnetic field which minimize the effect of magnetic field fluctuations for different francium isotopes. The experiment can be made not only between the $|F = 4, m_1\rangle, |F = 5, m_2\rangle$ levels, but also between the $|F = 4, m_2\rangle, |F = 5, m_1\rangle$ levels, that is, interchanging m_1 and m_2 , without changing anything except the state preparation where on the last step we would need to move into the other hyperfine level. The operating point of the static magnetic field and the frequency of the microwave cavity would have to be corrected slightly because of the nuclear spin contribution. Swapping m_1 and m_2 does not work as a reversal because the transition amplitudes change, but it can still be useful as a consistency check.

The frequency for the $F=4, m=0$ to the $F=5, m=-1$ transition in ^{209}Fr , expanded around the critical field $B_0 = 1553$ Gauss, is

$$\nu_m = 42.816 \times 10^9 + 90(B - B_0)^2 \text{Hz}, \quad (20)$$

where B is in Gauss. Under this scheme, control of the magnetic field to 0.06 Gauss (three parts in 10^5) reduces the frequency noise due to magnetic field fluctuations down to $\Delta\nu_m \sim 0.3$ Hz.

Even though the experiment takes place in a large magnetic field, the state preparation and detection have to be done in a small magnetic field. The transition between both regimes has to be done adiabatically, and care should be taken to avoid eddy current or hysteresis effects.

D. M1 transition

The dominant transition between the two hyperfine states is a magnetic dipole M1 transition. An M1 transition combined with other imperfections such as a misalignment of the polarization of the microwave field will

mimic the parity violating signal. In our proposal, the magnetic component of the microwave field drives these transitions. In this section, we examine ways to reduce M1 transitions between the two hyperfine states.

A microwave magnetic field polarized along the x axis has the same signature as a parity violating signal. The M1 transition amplitude between the levels of interest is given by

$$A_{M1}/\hbar = \langle \bar{f} | (-e/2m_e)(\mathbf{J} + \mathbf{S}) \cdot \mathbf{M} | \bar{i} \rangle / \hbar$$

$$= 7.8 \times 10^6 \left[\frac{M}{1.6 \text{ Gauss}} \right] \text{ rad}, \quad (21)$$

for the maximum expected microwave magnetic field in the Fabry-Perot cavity. The ratio of the E1 transition (Eq. 14) to the M1 transition is $|A_{E1}/A_{M1}| \sim 1 \times 10^{-9}$. Clearly, we need to carefully account for this transition or strongly reduce it. We choose to suppress it in three ways.

First (see Fig. 3(a)), we place the atoms at the magnetic field node (electric field anti-node) of the microwave cavity. If the dimension of the trap along the cavity axis is $d_t = 10 \mu\text{m}$, then the magnitude of the microwave magnetic field at the edges is reduced by a factor $\aleph = \sin(2\pi d_t/\lambda_m)$. At 45 GHz this gives a reduction factor of $\aleph = 4.8 \times 10^{-3}$.

Second (see Fig. 3(b)), we direct the polarization of the M1 field to be along the z -axis (Fig. 2). The M1 transitions in this case will be of the type $\Delta m = 0$, but the transition will not be resonant. The static magnetic field, B_{DC} , splits the magnetic sublevels of the two hyperfine levels, and the microwave field is resonant for the $|\Delta m| = 1$ E1 transitions (the microwave electric field is polarized along the x axis). The alignment will not be perfect and so we expect a suppression factor equal to $\sin(\phi) \sim \phi \sim 10^{-3}$, the angle of the microwave magnetic field polarization with respect to the z axis.

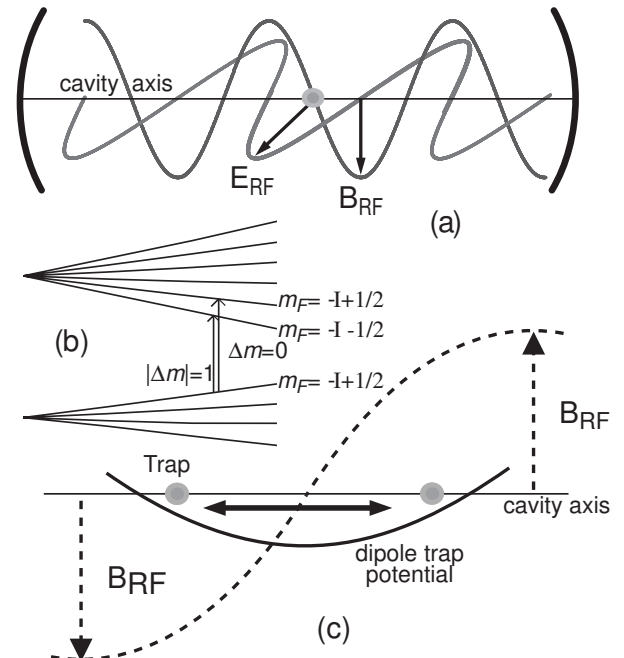


FIG. 3. Suppression mechanisms. (a) Trapped atoms sit at the magnetic field node, where the magnetic field is zero, (b) Schematic of the ground hyperfine levels showing a $|\Delta m| = 1$ transition such as the one for the anapole moment and the $\Delta m = 0$ transition such as that induced by the M1 field. This last one is out of resonance. The level spacing as well as the spin do not correspond to any particular atom. (c) Trapped atoms oscillate around the microwave magnetic field node and sample a zero time-averaged magnetic field.

Third (see Fig. 3(c)), the atoms in the dipole trap oscillate around the microwave magnetic field node. When an atom crosses the node, it sees a microwave magnetic field pointing in the opposite direction. The change in position effectively flips the phase of the magnetic field which the atom sees, and reverses the evolution of the transition so that the transition is dynamically suppressed. The suppression will only take place if the frequency of oscillation (ζ) of the atoms inside the trap is larger than the Rabi frequency of the M1 transition. The suppression factor is given by $(1/\sqrt{N})\Omega_{M1}/\zeta$. The frequency of oscillation along the cavity axis for our geometry is $\zeta/2\pi \sim 300 \text{ Hz}$.

Taken together, the three suppression mechanism reduce the expected M1 transition amplitude to $A_{M1s}/\hbar = 1.9 \times 10^{-5} \text{ rad}$ for 10^6 atoms. This is about 2×10^{-3} the amplitude for the E1 transition.

E. The microwave cavity

We must drive the anapole-induced hyperfine microwave transition at around 45 GHz. We choose to provide a standing wave microwave field with a Fabry-Perot cavity.

At this frequency, the wavelength of the excitation field

is $\lambda_m \sim 0.66$ cm. The cavity will have a mirror separation of $d \sim 20\lambda_m \sim 13$ cm. In order to minimize diffraction losses, we choose a mirror radius of $r_m=3.5$ cm, which gives a Fresnel number $F_N > 1$, where $F_N = r_m^2/\lambda_m d$ [28].

The expected quality factor (Q) of the cavity given by

$$Q = \frac{d}{2\zeta}, \quad (22)$$

where ζ is the skin depth and is equal to $\sqrt{2/\omega\mu_0\sigma}$ with μ_0 the magnetic constant and σ the conductivity which is $5.8 \times 10^7 \Omega^{-1}\text{m}^{-1}$ for copper at room temperature. For the Fabry-Perot cavity described above, the expected quality factor at 45 GHz is $Q = 1.9 \times 10^5$. With current available technology it is possible to couple 58 mW into the cavity which gives the 476 V/cm field used in the calculation of Eq. 14.

A waist of 1 cm for the cavity is enough to cover the 1mm diameter of the atom cloud. We choose a radius of curvature of $R_m=9.9$ cm for the cavity mirrors to ensure stable cavity, since for our parameters $(1 - (d/2R_m))^2 < 1$. Due to the curvature of the wavefronts the atoms will feel an small gradient on the polarization of the microwave field. The gradient is smaller than 3×10^{-5} rad cm^{-1} over the volume of the trap. Later, we will show that this rotation is within acceptable ranges and does not significantly affect the anapole moment measurement.

The field inside the cavity can be decomposed into a standing wave and a traveling wave. The presence of the travelling wave directly generates M1 transitions despite the location of the atoms at the node of the standing wave magnetic field. We can significantly reduce the amplitude of any intracavity travelling wave by adopting a symmetrical arrangement in which the microwave field is produced by two identical antennas, one on each mirror. The use of an antenna gives a very high coupling efficiency into the cavity [29] as compared to a slit or a grating [30]. The electric field inside the cavity is given by

$$E = e^{-i\nu_m t} \left(\frac{1}{1 - r_1 r_2 e^{2ik_m d}} \right) [E_1 t_1 (e^{ik_m z} - r_2 e^{ik_m d} e^{-ik_m z}) + E_2 t_2 (e^{-ik_m z} - r_1 e^{ik_m d} e^{ik_m z})], \quad (23)$$

where r is the reflectivity, t the transmissivity, k is the wave-vector of the microwave field, d the separation between the mirrors and the subindices 1 and 2 refer to the two mirrors. The first and second terms represent the field generated by the antenna 1 and 2 respectively. The expression is the sum of two waves, one travelling to the right and the other to the left. The difference in amplitude between these two contributions will result in a travelling wave. Assuming a symmetrical cavity, that is $r_1 = r_2 = r$ and $t_1 = t_2 = t$ the ratio of travelling to standing wave is

$$\mathcal{R}_{T/S} = \left(\frac{i\vartheta}{4} + \frac{E_1 - E_2}{4E_1} \right) (i(1 - r) + k_m \Delta d), \quad (24)$$

with ϑ the phase mismatch from both antennas and Δd the deviation of the cavity mirrors separation from the ideal position. Assuming $\vartheta = 0$ and that we can control the amplitude from each antenna to 1%, the position of the mirrors to $0.1 \mu\text{m}$ and taking $1 - r = 3.6 \times 10^{-4}$ (consistent with the Q factor computed above), we obtain $\mathcal{R}_{T/S} = (3 + 9i) \times 10^{-7}$.

F. Dipole trap

The atomic sample must remain trapped over the course of the measurement. We choose to use a far-detuned dipole trap, since the perturbations produced by these are small and measurable. A variety of different geometries have been proposed over the years. These include red-detuned traps based on focused beams, and blue-detuned traps with hollow beams (see Ref. [31,32] for reviews of recent work). In this section we examine the effect of a dipole trap on the anapole measurement.

We consider a dipole trap which confines the atomic sample to a volume with a $10 \mu\text{m}$ length along the cavity axis, and a 1 mm diameter in the radial dimension. The small axial dimension confines the atoms to the node of the magnetic microwave cavity field and therefore it has to be as small as experimentally possible. The transverse dimension should be smaller than the waist of the cavity field. The atoms are confined to a region smaller than the microwave wavelength (Lamb-Dicke regime) where the Doppler broadening becomes negligible. Since we will use up to 10^6 atoms for the measurement, the density of the atomic sample is 10^{11}cm^{-3} . The use of far detuned trap will prevent the appearance of light-assisted collisions.

The depth of the confining potential must be at least ten times the average temperature of the atoms to avoid losses through evaporation. The ground state AC Stark shift produced by far of resonance trap including only bound state contributions is given by [16]

$$\Delta E = -\frac{e^2 E_0^2}{4m} \left[\sum_e \frac{f_e}{\omega_e^2 - \omega^2} \right], \quad (25)$$

where $\hbar\omega_e$ is the excited state energy and f_e is the oscillator strength. Fig. 4 shows a calculation of the intensity required for a trap depth of 10kT ($T=1 \mu\text{K}$, as expected for molasses in Fr.). Only the 7p levels are included in the summation with linear polarization and they correspond to the zero crossings in the figure.

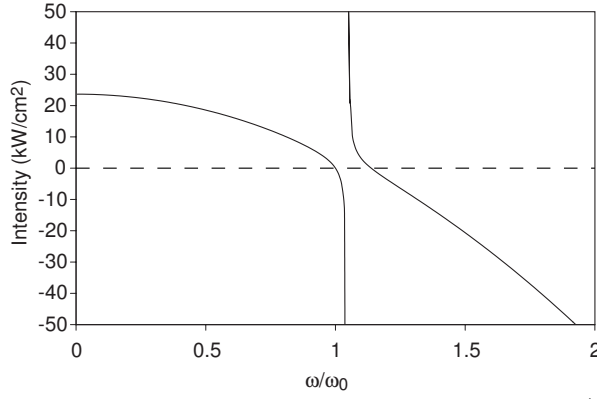


FIG. 4. Intensity required for a wall of height 10kT (10 μ K) for ^{209}Fr . The frequency is normalized to $\omega_0 = 2.3 \times 10^{15}$ rad/s the frequency of the $7P_{1/2}$ level ($\lambda_0 = 817$ nm). Negative intensity indicates that the trap is blue detuned).

The AC Stark shift, which produces the confining force of the dipole trap, displaces the two hyperfine levels of ground state in the same direction but not by the same amount. This differential shift changes the resonant frequency for the cavity-driven E1 transition used in the anapole moment measurement. For a detuning ($\delta = w - w_e$) larger than the hyperfine splitting (Δ_{HFS}) the change in the hyperfine separation is approximately equal to $(\Delta_{HFS}/\delta)\Delta E$ [33]. The advantage of using a far of resonance trap (FORT) is that we can reduce this shift considerably.

The atoms in the trap will occupy different vibrational levels. For a sufficiently far detuned trap transitions between different vibrational levels are suppressed. Each vibrational level has slightly different resonance frequency which will lead to broadening of the signal and loss of coherence. One possible solution is to superimpose an additional laser to the trap that produces a differential Stark shift that exactly cancels the one for the trap. This can be achieved by tuning the laser frequency exactly in the middle of the ground hyperfine levels and adjusting the intensity accordingly [33]. The problem with this technique is that the photon scattering will still be present.

Another option is to use a blue detuned trap such that the atoms spend more time in the dark. Coherence times as long as 4.4 s have been proven with a blue detuned trap, this is 300 times larger than the coherence time obtained with a red detuned trap under similar conditions [34]. The main source for decoherence in this case is distribution of Stark shifts felt by the atoms.

Using a laser at 532nm we expect a coherence time 16 times smaller in francium because of the difference in hyperfine splittings and detunings. The dephasing grows slowly in time and can be reversed with the use of an “echo” technique. We can increase the magnitude of the Raman pulse to $(2n + 1)\pi/2$ such that the atoms spend half of the time in each hyperfine level. In this case we only need to keep the coherence for a time approximately equal to t_c/n with t_c the coherence time. Using $n=38$ we

only need a coherence time of 26 ms to have an interaction time of 1s. This is below the expected 300 ms coherence time.

The atoms will oscillate between the dark and bright regions of the trap and on the walls they will see an average differential Stark shift approximately equal to $kT(\Delta_{HFS}/\delta)/h=6.3$ Hz. The effect of this time varying detuning is similar to a steady state detuning of the same magnitude. Since this can be compensated by changing slightly the microwave frequency then we only care about changes on the maximum detuning.

The dipole trap in combination with the cavity field may generate a multi-photon transition. There are four vectors involved in such transition: $\mathbf{E1_D}$, $\mathbf{M1_D}$ the dipole trap electric and magnetic fields, \mathbf{E} the microwave electric field and \mathbf{B} the static magnetic field. We can form two parity and time reversal conserving observables: $(\mathbf{E1_D} \cdot \mathbf{E})(\mathbf{M1_D} \cdot \mathbf{B})$ and $(\mathbf{E1_D} \cdot \mathbf{B})(\mathbf{M1_D} \cdot \mathbf{E})$. For both cases having the dipole laser propagation perpendicular to the cavity axis will bring their contributions to negligible levels.

IV. TECHNICAL NOISE

We can measure the anapole moment by determining the population transferred from the lower hyperfine level to the upper hyperfine level by the application of the Raman and microwave fields. Both of these fields (or any other stray field) are characterized by a field amplitude, frequency (or detuning), and interaction time. We will assume a common detuning (δ) and interaction time (t). The total transition amplitude will be given by

$$A = (A_{R1} + A_{E11} + A_1) + i(A_{R2} + A_{E12} + A_2), \quad (26)$$

where $A_{R1,R2}$ are the real and imaginary components of the Raman amplitude, $A_{E11,E12}$ the corresponding for the E1 transition amplitude and $A_{1,2}$ are the real and imaginary parts of any other transition present such as an M1 transition.

Table II shows the phase of the different type of transitions for different field polarizations. This table also shows which transitions change sign under magnetic field reversal. Some fields have an additional phase factor, so for example the E1 amplitude inside the cavity has to be multiplied by $e^{i\psi}$, the standing wave M1 field inside the cavity is out of phase with the E1 so it has to be multiplied by $ie^{i\psi}$, and if we have a travelling wave M1 transition generated by the microwave cavity then it has to be multiplied by $e^{i\psi}$. ψ is an experimental knob that we can change to look for systematic effects.

The Raman field will be polarized along the y axis so that $A_{R1} = A_{Ry}$ and the E1 transition is polarized along the x axis so that $A_{E11} = iA_{E1x}$ (or $\psi = \pi/2$). These two amplitudes will interfere since both are in phase and

only one (the E1) changes sign under magnetic field reversal as shown in Table II. Expanding Eq. 15 for large A_{Ry} and everything else small we obtain

$$\Xi = \sin^2\left(\frac{A_{Ry}t_R}{2\hbar}\right) + \frac{1}{2}\sin\left(\frac{A_{Ry}t_R}{\hbar}\right)\left(\frac{A_{eff}t_R}{\hbar}\right),$$

$$A_{eff} = \left(iA_{Ex} + A_1 + \frac{\hbar^2\delta^2}{2A_{Ry}} + \frac{1}{A_{Ry}}(A_{Rx} + A_2)^2\right). \quad (27)$$

The signal and noise terms are contained in A_{eff} . We can use this expression to set limits in the different experimental parameters. This expression can also be used to identify the corresponding observable, for example, expanding the expression for small t we obtain for the first term in A_{eff} something proportional to $iA_{Ry}A_{E1x}$ which corresponds to the PNC signal $\mathbf{i}(\mathbf{E} \times (\mathbf{E}_{R1} \times \mathbf{E}_{R2})) \cdot \mathbf{B}$ (the magnetic field \mathbf{B} keeps time reversal symmetry).

We will divide the analysis into three parts: Line broadening mechanisms which contain terms that induce some noise in the experiment that averages to zero after an infinite number of cycles, systematic effects that include terms that mimic the PNC signal, and calibration errors that modify the value of the extracted constants on the PNC signal.

A. Line broadening mechanisms

In this section we will show the requirements for a 3% measurement on the terms that do not change under reversal. The corresponding terms in the last parenthesis of Eq. 27 have to be controlled to $3A_{E1}$ for 10^4 repetitions.

1. A_{Ry}

From Eq. 27 we see that the effect of some of the noise terms will be reduced if we increase A_{Ry} as much as possible. We can take A_{Ry} to be exactly equal to a $(2n+1)\pi/2$ pulse, and we include any deviation from this value into A_1 . We can control the Raman pulse to 0.025% in one second if we are shot noise limited. In this case the maximum value we can have for the Raman pulse is $A_{Ry}/\hbar = 121$ rad or $n = 38$.

2. δ

The detuning has to be controlled to $\delta = 2.7$ rad. The required accuracy for the microwave field frequency is one part in 10^{11} .

The Raman $\pi/2$ pulse, which initially prepares the atoms, consists of two laser fields. Both of these must be phase locked with respect to each other, but also with respect to the microwave field. This is technologically feasible with diode lasers [35,36]. If necessary the Raman

pulse can be substituted by an M1 pulse generated by a microwave horn. The advantage of using an M1 is that the field will be automatically phase locked with the E1 transition because both come from the same microwave source.

The dipole trap shifts the levels but as we just showed earlier, as long as the trap is sufficiently far detuned the effects can be reduced. For a trap at 532 nm the Stark shift will be 6.3 Hz. This shift (or the dipole laser power) has to remain constant to 7% to be below the limit set before.

The presence of an M1 transition will produce an AC shift of the levels. The value of the maximum shift is ~ 3 mHz which is negligible.

For what follows we will ignore the detuning and we will concentrate only in the amplitudes involved in the experiment. The amplitudes of interest are the Raman amplitudes $A_{Rx,Ry}$, the E1 amplitude A_{E1x} , an M1 transition that is in phase with the E1 field $A_{Mix,Miy}$ and an M1 transition that is $\pi/2$ out of phase with the E1 field $A_{Mox,Moy}$. As an example, if the standing wave magnetic field inside of the cavity is tilted towards the x axis it will generate an amplitude A_{Mox} since this field will be out of phase with the E1 field. The M1 amplitudes are included into Eq. 27 as A_1 or A_2 depending on their phase relation to A_{Ry} .

The most interesting values for the relative phase (ψ) between the E1 and the Raman transition are multiples of $\pi/2$. First we will study the case with $\psi = 0, \pi$. This does not correspond to the PNC measurement since the E1 transition and the Raman transition will be out of phase and therefore they will not interfere. The signal obtained with this configuration will be helpful in the evaluation of unwanted contributions. Using Table II we can rewrite A_{eff} from Eq. 27 as

$$A_{eff} = \frac{1}{A_{Ry}} [(A_{Mox}^2 - A_{Miy}^2 - A_{Rx}^2) + s(iA_{Ry}A_{Moy} - 2iA_{Rx}A_{Mox}) + \beta(-2iA_{Miy}A_{Mox}) + s\beta(A_{Ry}A_{Mix} - 2A_{Miy}A_{Rx})], \quad (28)$$

with $s = 1, -1$ when $\psi = 0, \pi$ respectively and $\beta = 1, -1$ depending if we have the normal experiment or we apply a magnetic field reversal. With $\psi = \pi/2, -\pi/2$ instead we get

$$A_{eff} = \frac{1}{A_{Ry}} [(A_{Mix}^2 - A_{Rx}^2 - A_{Moy}^2) + s(iA_{Ry}A_{Miy} + 2iA_{Rx}A_{Mix}) - \beta(-2iA_{Moy}A_{Mix}) + s\beta(2A_{Rx}A_{Moy} - A_{Ry}A_{Mox} + iA_{Ry}A_{E1x})], \quad (29)$$

where now $s = 1, -1$ when $\psi = \pi/2, -\pi/2$ respectively. This corresponds to the experimental condition for the PNC measurement. The PNC signal is contained in the last term, and it changes sign under both reversals as it should. This is how reversals can be used to isolate

the signal from other contributions. The other terms that have the same behavior under reversals constitute the systematic effects and these are the most dangerous terms. We continue with the analysis of the terms that do not have the same behavior under reversals and can be isolated.

$$3. A_{Rx}^2/A_{Ry}$$

This term appears due to a bad polarization alignment of the Raman field. If we assume that the polarization of the Raman field can be adjusted to one part in 10^3 then this requirement is fulfilled.

$$4. isA_{Ry}A_{Miy}/A_{Ry}$$

Most of the terms that depend on the M1 transition are multiplied by an small number such as A_{Rx}/A_{Ry} . This is not the case for this term so we must understand its origin and magnitude.

The magnetic microwave field inside the cavity is out of phase with respect to the electric field because it is an standing wave. Imperfections on the standing wave may create travelling wave components that may be in or out of phase with respect to the microwave electric field.

Eq. 24 gives the amplitude of the travelling wave expected in our setup. The travelling wave is polarized along the z axis, so we can include the polarization suppression factor of 10^{-3} . Combining these two numbers with the amplitude for the M1 transition we get an amplitude which is $0.25A_{E1}$ and is out of phase with the E1 transition or an amplitude of $0.75A_{E1}$ which is in phase. This is enough for the requirement of $A_{Miy} < 3A_{E1x}$.

The relative phase between both antennas (ϑ) can be adjusted by minimizing the M1 contribution when the magnetic field is tilted slightly. The antennas phase mismatch contribution will be smaller than the one just mentioned if $\vartheta < 0.01$ rad.

B. Systematic effects

The constraint in the terms that mimic the PNC signal is stronger since these terms do not average out. To get a 3% measurement their contribution must be below $0.03A_{E1}$.

$$1. s\beta A_{Rx}A_{Moy}/A_{Ry}$$

This term appears because of a combination of misalignment of the Raman field, misalignment of the microwave field, or imperfections in the microwave cavity as shown before. It corresponds to the observable

$(\mathbf{M} \times (\mathbf{E}_{R1} \times \mathbf{E}_{R2})) \cdot \mathbf{B}$. Since this term is reduced by the Raman misalignment its contribution becomes negligible.

$$2. s\beta A_{Ry}A_{Mox}/A_{Ry}$$

This term has the same origin as the previous one, but now its contribution is considerably larger since now is multiplied by A_{Ry} . This is the most dangerous term and eventually the limiting factor in the precision of the measurement. To reduce this term one depends completely on the suppression mechanisms. For a 3% measurement we must maintain the suppression mechanisms to that level also.

The cavity mirrors may have some birefringence, which will generate a microwave magnetic x -axis component. For the cavity we have considered, the microwaves make roughly 100 reflections. To keep the M1 suppression the same then we want a polarization rotation smaller than 10^{-3} rad, the rotation per reflection must be smaller than 10^{-5} rad. If the other suppression mechanisms work properly this constraint can be relaxed by a factor of 14 and still get a 3% measurement.

The atomic sample must be precisely held at the node of the microwave magnetic field. The maximum displacement we can tolerate is 3×10^{-11} m to keep the 3% measurement.

C. Calibration errors and extraction of nuclear physics

Once we isolate the PNC signal (Eq. 16) it is necessary to extract the constants of the interaction from it. The uncertainty in the Raman amplitude and interaction time are negligible, then from the measurement we get directly A_{E1}/\hbar . The amplitude is the product of the microwave electric field and the matrix element. The microwave electric field has to be known to 3%. The electric field can be measured by tilting the magnetic field and inducing an M1 transition. The wave functions used on the matrix element have to be also known to the same accuracy to extract κ_{nsd} . The effective constant of the anapole moment κ_a can be obtained after subtracting the other two contributions to κ_{nsd} (Eq. 4). As explained before, the anapole moment of the even-neutron isotopes comes only from the unpaired proton, while the odd-neutron isotopes contain contributions from the unpaired proton and neutron. A measurement of the anapole moment to better than 10% will give an initial separation of both contributions. The effective constant of the anapole moment is related to the weak meson-nucleon couplings, and the measurement will further constrain their values [19]. Furthermore, the constraints obtained with the odd and even neutron isotopes are almost orthogonal on the

meson-nucleon coupling space [4]. Extraction and understanding of the nuclear parameters will require an equivalent effort from theorists to improve their calculations of both the atomic and nuclear physics involved.

D. Other sources of fluctuations

Transitions to other levels are generated by the microwave magnetic field. These are transitions of the type $\Delta m = 0$ but they are small because they are non-resonant at the magnetic field we will be working (detuning ~ 0.4 GHz). Nevertheless, these transitions must still be taken into account in a detailed analysis of the data.

The presence of stray electric fields produces Stark induced transitions that mimic the PNC signal. A stray electric field of a magnitude of 13 V/cm in the z direction will generate a transition amplitude equal to the parity violating signal. Stray fields large enough to be a problem are unlikely to occur and can be ignored [27].

Gradients can also induce higher order multipole transitions such as an E2 transition or an even higher transition. Fortunately, these higher order transition between the two hyperfine ground levels are strongly suppressed. Table III summarize the results of the above analysis of systematic effects.

V. CONCLUSION

The anapole moment provides a unique probe of weak hadronic interactions. In particular it is sensitive to weak long range meson exchange interactions, and consequently allows a measurement of weak neutral currents in the nucleus. This is not the case in high energy experiments where the weak contribution must be separated from the strong and electromagnetic contributions which are much larger. We have presented the analysis of a measurement strategy of the nuclear spin dependent part of the PNC interaction, dominated by the anapole moment. While the proposed measurement method can be extended to other alkali atoms, a series of measurements in a chain of francium isotopes will allow the separation of the proton and neutron contributions to the anapole moment. The production and trapping of sufficient amounts of francium is necessary to obtain a precise measurement. The contributions from protons and neutrons will permit stronger orthogonal constraints on meson-nucleon couplings.

ACKNOWLEDGMENTS

Work supported by NSF. E. G. acknowledges support from CONACYT.

-
- [1] M.-A. Bouchiat and C. Bouchiat, Rep. Prog. Phys. **60**, 1351 (1997).
 - [2] Y. B. Zel'dovich, Sov. Phys.-JETP **9**, (1959).
 - [3] V. V. Flambaum, I. B. Khriplovich, and O. P. Sushkov, Phys. Lett. B **146**, 367 (1984).
 - [4] W. C. Haxton and C. E. Wieman, Annu. Rev. Nucl. Part. Sci. **51**, 261 (2001).
 - [5] W. R. Johnson, M. S. Safronova, and U. I. Safronova, Phys. Rev. A **67**, 062106 (2003).
 - [6] Y. B. Zel'dovich, Sov. Phys.-JETP **6**, (1957).
 - [7] P. A. Vetter, D. M. Meekhof, P. K. Majumder, S. K. Lamoreaux, and E. N. Fortson, Phys. Rev. Lett. **74**, 2658 (1995).
 - [8] C. S. Wood, S. C. Bennett, D. Cho, B. P. Masterson, J. L. Roberts, C. E. Tanner, and C. E. Wieman, Science **275**, 1759 (1997).
 - [9] C. S. Wood, S. C. Bennett, J. L. Roberts, D. Cho, and C. E. Wieman, Can. J. Phys. **77**, 7 (1999).
 - [10] C. E. Loving and P. G. H. Sandars, J. Phys. B **10**, 2755 (1977).
 - [11] V. G. Gorshkov, V. F. Ezhov, M. G. Kozlov, and A. I. Mikhailov, Sov. J. Nucl. Phys. **48**, 867 (1988).
 - [12] D. Budker, in *Physics Beyond the Standard Model*, edited by P. Herczeg, C. M. Hoffman, and H. V. Klapdor-Klinckrothaus (World Scientific, Singapore, 1998).
 - [13] V. E. Balakin and S. I. Kozhemyachenko, JETP Lett. **31**, 297 (1980).
 - [14] V. N. Novikov and I. B. Khriplovich, JETP Lett. **22**, 74 (1975).
 - [15] J. S. Grossman, L. A. Orozco, M. R. Pearson, J. E. Sim-sarian, G. D. Sprouse, and W. Z. Zhao, Phys. Rev. Lett. **83**, 935 (1999).
 - [16] M. V. Romalis and E. N. Fortson, Phys. Rev. A **59**, 4547 (1999).
 - [17] C. Chin, V. Leiber, V. Vuletic, A. J. Kerman, and S. Chu, Phys. Rev. A **63**, 033401 (2001).
 - [18] I. B. Khriplovich, *Parity Non-Conservation in Atomic Phenomena* (Gordon and Breach, New York, 1991).
 - [19] V. V. Flambaum and D. W. Murray, Phys. Rev. C **56**, 1641 (1997).
 - [20] N. Fortson, Phys. Rev. Lett. **70**, 2383 (1993).
 - [21] S. G. Porsev and M. G. Kozlov, Phys. Rev. A **64**, 064101 (2001).
 - [22] C. Bouchiat and C. A. Piketty, Phys. Lett. B **269**, 195 (1991).
 - [23] E. A. Hinds and V. W. Hughes, Phys. Lett. B **67**, 487 (1977).
 - [24] E. G. Adelberger, T. A. Traino, E. N. Fortson, T. E. Chupp, D. Holmgren, M. Z. Iqbal, and H. E. Swanson, Nucl. Instrum. Meth. **179**, 181 (1981).
 - [25] S. Aubin, E. Gomez, L. A. Orozco, and G. D. Sprouse, Rev. Sci. Instrum. **74**, 4342 (2003).
 - [26] W. M. Itano, J. C. Begquist, J. J. Bollinger, J. M. Gilligan, D. J. Heinzen, F. L. Moore, M. G. Raizen, and D. J. Wineland, Phys. Rev. A **47**, 3554 (1993).

- [27] D. DeMille and M. G. Kozlov, arXiv: **physics**, 9801034 (1998).
- [28] S. Ramo, J. F. Whinnery, and T. V. Duzer, *Fields and Waves in Communication Electronics* (John Wiley and Sons, New York, 1993).
- [29] R. N. S. N. K. S. U. Harbarth, J. Kowalski and G. Z. Putlitz, J. Phys. E. Sci. Instrum. **20**, 409 (1987).
- [30] J. W. Dees and A. P. Sheppard, IEEE Trans. Inst. Meas. **14**, 52 (1965).
- [31] V. I. Balykin, V. G. Minogin, and V. S. Letokhov, Rep. Prog. Phys. **63**, 1429 (2000).
- [32] N. Friedman, A. Kaplan, and N. Davidson, Advances in Atomic, Molecular, and Optical Physics **48**, 99 (2002).
- [33] A. Kaplan, M. F. Andersen, and N. Davidson, Phys. Rev. A **66**, 045401 (2002).
- [34] N. Davidson, H. Lee, C. S. Adams, M. Kasevich, and S. Chu, Phys. Rev. Lett. **74**, 1311 (1995).
- [35] G. Santarelli, A. Clairon, S. N. Lea, and G. M. Tino, Opt. Commun. **104**, 339 (1994).
- [36] P. Bouyer, T. L. Gustavson, K. G. Haritos, and M. A. Kasevich, Opt. Lett. **21**, 1502 (1996).
- [37] A. Coc, C. Thibault, F. Touchard, H. T. Duong, P. Juncar, S. Liberman, J. Pinard, J. Lermé, J. L. Vialle, S. Büttgenbach, A. C. Mueller, A. Pesnelle, and the ISOLDE Collaboration, Phys. Lett. B **163B**, 66 (1985).
- [38] A. Coc, C. Thibault, F. Touchard, H. T. Duong, P. Juncar, S. Liberman, J. Pinard, M. Carre, J. Lerme, J. L. Vialle, S. Büttgenbach, A. C. Mueller, A. Pesnelle, and the ISOLDE Collaboration, Nucl. Phys. A **468**, 1 (1987).

Isotope	Spin	Hfs(MHz)	m ₁	m ₂	B ₀ (Gauss)	ν _m (Mhz)
208	7	49880.3	0.5	1.5	2386.5	49433
209	9/2	43033.5	0	-1	1553.0	42816
210	6	46768.2	0.5	1.5	2586.4	46208
211	9/2	43569.5	0	-1	1572.3	43349
212	5	49853.1	0.5	1.5	3265.7	49015

TABLE I. Parameters of the five relevant francium isotopes. This includes spin, hyperfine splitting (Hfs) of the $7s_{1/2}$ state [37,38], Zeeman sublevels m_1, m_2 , static magnetic field B_0 at the minimum hyperfine separation, and corresponding hyperfine separation ν_m at that magnetic field.

Reversal	m1	m2	P_{E1x}	P_{M1x}	P_{M1y}	P_{Rx}	P_{Ry}
Normal	0	-1	i	1	i	i	1
β	0	1	-i	-1	i	-i	1

TABLE II. Phase ($P = A/|A|$) of the relevant transition amplitudes for the initial state F1=4, m1 and final state F2=5, m2 and polarized along the specified axis. For this table all the fields have the same phase (equal to 0). P_{Rx} represents the Raman transition with one vector along the z axis and the other along the y axis such that their cross product points along the x axis. β represents the static magnetic field reversal together with a sign change on the Zeeman sublevel m .

Observable	Constraint	Set value	Stability
$A_{Ry}A_{E1}$	Microwave amplitude	476 V/cm	0.03
$A_{Ry}A_{Ry}$	Raman amplitude	121 rad	2.5×10^{-4}
$(\hbar\delta)^2$	Microwave frequency	45 GHz	10^{-11}
	Dipole trap Stark shift	6.3 Hz	0.07
	DC Magnetic field	1500 Gauss	4.7×10^{-5}
$A_{Rx}A_{Rx}$	Raman polarization	0 rad	10^{-3} rad
$A_{Ry}A_{Miy}$	Mirror separation	13 cm	7.7×10^{-7}
	Antenna power	57 mW	0.02
	Antenna phase	0 rad	0.01 rad
$A_{Ry}A_{Mox}$	Mirror birefringence	0 rad	1×10^{-4} rad
	Trap displacement	0 m	3×10^{-11} m

TABLE III. Fractional stability required for a 3% measurement. The observable associated with each constraint is also included.